Arabian Journal of Chemistry (2020) **13**, 4513–4527

King Saud University

Arabian Journal of Chemistry

www.ksu.edu.sa
www.sciencedirect.com

ORIGINAL ARTICLE

Controlled release formulation of zinc hydroxide nitrate intercalated with sodium dodecylsulphate and bispyribac anions: A novel herbicide nanocomposite for paddy cultivation

Sharifah Norain Mohd Sharif [a], Norhayati Hashim [a,b,*], Illyas Md Isa [a,b], Suriani Abu Bakar [b,c], Mohamad Idris Saidin [a], Mohamad Syahrizal Ahmad [a], Mazidah Mamat [d], Mohd Zobir Hussein [e]

[a] *Department of Chemistry, Faculty of Science and Mathematics, Universiti Pendidikan Sultan Idris, 35900 Tanjong Malim, Perak, Malaysia*
[b] *Nanotechnology Research Centre, Faculty of Science and Mathematics, Universiti Pendidikan Sultan Idris, 35900 Tanjong Malim, Perak, Malaysia*
[c] *Department of Physics, Faculty of Science and Mathematics, Universiti Pendidikan Sultan Idris, 35900 Tanjong Malim, Perak, Malaysia*
[d] *School of Fundamental Science, Universiti Malaysia Terengganu, 21030 Kuala Terengganu, Terengganu, Malaysia*
[e] *Materials Synthesis and Characterization Laboratory, Institute of Advanced Technology, Universiti Putra Malaysia, 43400 Serdang, Selangor, Malaysia*

Received 5 July 2019; accepted 24 September 2019
Available online 3 October 2019

KEYWORDS

Nanocomposite;
Bispyribac;
Zinc hydroxide nitrate;
Sodium dodecylsulphate;
Intercalation

Abstract Bispyribac (BP) anions have been successfully intercalated in the interlayer region of zinc hydroxide nitrate (ZHN) in the presence of sodium dodecylsulphate (SDS) surfactant. The physicochemical properties of the intercalation compound ZHN–SDS–BP have been characterised herein with different instrumental techniques. The intercalation of BP and SDS is clearly reflected in the PXRD analysis, based on the appearance of symmetrical, sharp and intense intercalation peaks at lower 2θ with a basal spacing of 28.2–28.6 Å. The thermal studies show that the ZHN–SDS–BP nanocomposite has better thermal stability than the pristine BP. The intercalation of BP leads

* Corresponding author at: Department of Chemistry, Faculty of Science and Mathematics, Universiti Pendidikan Sultan Idris, 35900 Tanjong Malim, Perak, Malaysia.
E-mail address: norhayati.hashim@fsmt.upsi.edu.my (N. Hashim).
Peer review under responsibility of King Saud University.

Production and hosting by Elsevier

https://doi.org/10.1016/j.arabjc.2019.09.006

to significant changes in the surface area, porosity, and morphology. Nitrogen adsorption–desorption isotherms reveal that both ZHN–SDS and ZHN–SDS–BP are of Type IV. The release and kinetic studies were also carried out on the ZHN–SDS–BP, in aqueous solution of Na_3PO_4, Na_2SO_4 and NaCl as the release media. The releases of BP in both aqueous solutions of Na_3PO_4 and NaCl were found to follow the pseudo second order kinetic model, whereas the releases of BP in the aqueous solution of Na_2SO_4 obey the parabolic diffusion kinetic model. This study shows that ZHN has the potential to be used as a host material in slowing the release of BP herbicides in the paddy cultivation sector.

1. Introduction

Layered hydroxide salts (LHS) are a type of layered material with an anion exchange capacity, and have a structure made up of only one divalent metal cation. LHS are represented by the general formula of $M^{2+}(OH)_{2-x}(A^{m-})_{x/m}{\cdot}nH_2O$, where M^{2+} represents the metal cation and A^{m-} refers to the guest anion (Fernandes et al., 2014). There are many possible combinations of metal cation and guest anion, according to the preparation method.

Zinc hydroxide nitrate (ZHN) is a LHS variant that has been widely used as a host material for various guest anions such as adipate, azelate, and benzoate (Arizaga et al., 2008). The structure of ZHN originates from brucite ($Mg(OH)_2$), but with a slight modification. One quarter of the octahedrally coordinated zinc in the structure is relocated from the main layer to the tetrahedral site; positioned above and below each of the empty octahedra. Exchangeable NO_3^- are surrounded by water molecules and located in the interlayer, where they are not directly bonded to the central zinc atoms (Cordeiro et al., 2008). The thermodynamically favourable transition forming the ZHN from the aqueous zinc nitrate solution has been reported in recent studies (Moezzi et al., 2013). The reaction is thermodynamically controlled by the concentration of cationic zinc species, $ZnOH^+$ produced by dissolution of ZnO in the acidic solution of zinc nitrate. A reliable qualitative agreement that was established between theoretical and experimental data using various methods in determining the thermodynamic compatibility related to the formation of nanocomposites have also been reported (Bravo-Suárez et al., 2004; He et al., 2006; Rana et al., 2000, 1996a, 1996b, 1993).

The implementation of intercalation is a significant area of interest, considering that it entraps a guest ion in the interlayer gallery of the layered material, thus enabling the alteration of the original properties as a consequence of changes in electron density (Jaerger et al., 2014). Theoretically, the layered host materials can adapt to the geometry of the intercalated guest ion by modification of the interlayer spacing. Even though the layered host materials possess strong intralayer covalent bonds, the interlayer interactions are weak, which allows guest ions with suitable functional groups to self-assemble into mono- or bilayers between the sheets of the layered host material (Nhlapo et al., 2008). Phenylalanine, isocoumarin, ochratoxin A, α-alanine, gibbsite and 5-aminosalicylic acid are few examples of guest ions that have been intercalated into the host material to form nanocomposites (Hong et al., 2014; Rees et al., 2014; Ribeiro et al., 2014; Soledad et al., 2015).

Several studies have reported on the important role of surfactants in assisting the intercalation process (Liu et al., 2015; Nhlapo et al., 2008; Qiu et al., 2009; Zhenlan et al., 2009). The presence of surfactants is reported to enlarge the interlayer spacing of the layered materials; hence, it is easier to entrap the guest anion (Tao et al., 2009). Some of the intercalated guest ions that were reported to be successfully intercalated into the interlayer gallery of the host, in the presence of surfactants include salicylates, cinnamates, benzophenone, chlorpyrifos, hexaconazole, and triadimenol (Cristina et al., 2013; Liu et al., 2015; Pesquisa et al., 2015; Zhenlan et al., 2009).

The intercalation of herbicide guest ions into a suitable host is a promising way to introduce controlled release formulation (CRF) to a conventional herbicide, as an endeavour for overcoming excessive herbicide usage in the environment (Bruna et al., 2009; Hussein et al., 2011; Touloupakis et al., 2011). The continuous usage of conventional herbicides in the long term will cause a considerable portion of herbicide residues to be released into surface and ground waters through numerous possible processes, including sorption, degradation, runoff and leaching. This therefore leads to water and soil pollution that will eventually harm living organisms. Unlike conventional herbicides, herbicides with CRF, allowing the slow release of herbicide into the environment, subsequently reduce the non-target effects and minimise the risk of pollution.

Bispyribac (BP), which is commercialised as bispyribac-sodium and also known as sodium 2,6-bis(4,6-dimethoxypyrimidin-2-yloxy)benzoate, is a white powder herbicide used to control common barnyard grass and numerous floating, submersed and emergent weeds found in paddy cultivation areas, such as water hyacinth and hydrilla (Durborow, 2014). The chemical structure of BP is shown in Fig. 1. This herbicide exterminates weeds systemically by preventing the action of a key amino acid-synthesizing enzyme, acetolactate synthase (Chauhan and Johnson, 2010).

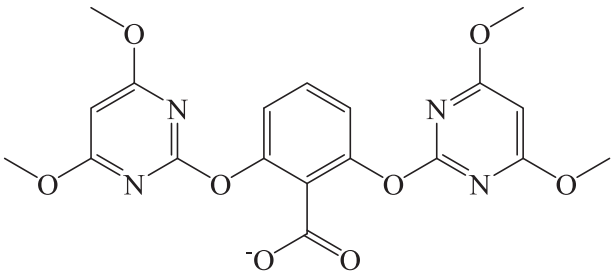

Fig. 1 The Chemical Structure of Bispyribac.

Owing to the fact that it is possible for the BP to enter into the food chain and trigger the carcinogenic and mutagenic effects on the living organisms, the commercial formulation containing BP is considered to be lethal (Lajmanovich et al., 2013; Ruiz de Arcaute et al., 2016; Toni et al., 2010; Zhang et al., 2013). Hence, various approaches have been proposed to overcome the environmental issues originated from the extensive use of BP. These include monitoring the concentration of BP residues in the soil, developing new methods to improve the effectiveness of BP degradation and investigating the effect of organic matter and clay content on the adsorption of BP (Ahmad et al., 2019, 2018; Almalike et al., 2015; Galla et al., 2019; Qamruzzaman and Nasar, 2019). Despite the variety of approaches proposed in previous research, no research has yet been reported on the implementation of CRF in minimising the pollution caused by BP.

In this study, BP was selected to be intercalated into the interlayer gallery of ZHN, in the presence of the surfactant sodium dodecylsulphate (SDS). The possibility of using the zinc hydroxide nitrate–sodium dodecylsulphate–bispyribac (ZHN–SDS–BP) nanocomposite in CRF applications were further experimented using sodium phosphate (Na_3PO_4), sodium sulphate (Na_2SO_4) and sodium chloride (NaCl) as release media. To the best of our knowledge, this research is the first evidence for the intercalation of BP into a ZHN host and their application in CRF field. The novel synthesised nanocomposite herein, is hopefully will benefit the paddy cultivation sector in the future.

2. Experimental methods

2.1. Reagents

The main reagents, $Zn(NO_3)_2{\cdot}6H_2O$ (purity 98%) and sodium dodecylsulphate (SDS) were both purchased from Systerm. The intercalated guest anion BP was bought from China (purity 98%). The NaOH and HCl that were used to adjust the pH of the solutions were obtained from Merck and Sigma-Aldrich, respectively. Deionised water was used to prepare all solutions, and all reagents were used as received, without further purification.

2.2. Synthesis of ZHN–SDS–BP nanocomposite

The ZHN–SDS–BP nanocomposite was synthesised by following the method described in (Liu et al., 2015). ZHN was initially intercalated with SDS by co-precipitation, so as to synthesise the ZHN–SDS nanocomposite. A solution (40 ml) with 10 mmol of SDS was prepared and later reacted with 40 ml of 20 mmol $Zn(NO_3)_2{\cdot}6H_2O$ and 1 M NaOH. The reaction was performed at room temperature in a nitrogen atmosphere and continuously stirred. The pH was adjusted to a value of 6.5; a few drops of HCl were added to the mixture if necessary. The obtained white slurry was then aged at 70 °C in an oil bath shaker for 24 h and centrifuged at 40 rpm for 5 min. The precipitate collected was then oven dried at 60 °C and ground into fine powder.

In order to intercalate the guest anion BP into the synthesised ZHN–SDS, 50 ml of 0.02 mol·litre^{-1} BP solution was prepared by dissolving 1 mmol of BP in ethanol and deionised water. ZHN–SDS (0.3 g) was then dispersed into the BP solution along with a further 20 ml of deionised water. The mixture was stirred for 2 h and the slurry obtained was then aged for 24 h at 70 °C in an oil bath shaker. After ageing, the mixture was centrifuged at 40 rpm for 5 min to collect the precipitate. The ZHN–SDS–BP precipitate was oven dried at 60 °C, ground into a fine powder, and stored in sample bottles until characterisation. The same procedure was repeated using two further BP concentrations (0.05 and 0.1 M).

2.3. Characterisation

ZHN–SDS, BP, and ZHN–SDS–BP were characterised using a number of different instrumental procedures. Powder X-ray diffraction (PXRD) analyses were performed with a PANalytical X'pert Pro MPD, using Co Kα radiation (0.15406 nm) in the range of 2–60°. The measurement conditions were: step size, 0.0330°; scan step time, 19.4434 s; and generator settings, 30 mA, 40 kV. Fourier transform infrared (FTIR) spectra were recorded in the range of 400–4000 cm^{-1}, using KBr discs on a Nicolet from Thermo Electron Corporation. The thermogravimetric and derivative thermogravimetric analysis (TGA/DTG) was studied using a Perkin-Elmer Pyris 1 thermogravimetric analyser Thermo Balance with heating rate of 10 °C·min^{-1} in a nitrogen environment.

The determination of metal content was performed by inductively coupled plasma optical emission spectrometry (ICP-OES, model Perkin-Elmer Plasma 1000) after digesting the sample in HCl, whereas the amounts of carbon, nitrogen, and hydrogen in the sample were determined by a CHNS elemental analyser (model CHNS-932 LECO). Field emission scanning electron microscopy (FESEM) images were obtained using a Hitachi SU 8020 UHR instrument. The surface properties were analysed using a Quantachrome Autosorb automated gas sorption analyser, under nitrogen adsorption–desorption at 110.0 °C. The samples were outgassed for 10 h to eliminate the adsorbed species from the sample.

2.4. Herbicide release study

The release of BP from the interlayer gallery of the ZHN-SDS-BP nanocomposite was monitored by adding 0.6 mg of ZHN-SDS-BP into a cuvette containing 3.5 ml of aqueous salt solution. Three type of aqueous salt solutions were used as release media, Na_3PO_4, Na_2SO_4, and NaCl, each prepared with three different concentrations (0.3, 0.5 and 1.0 M). The quantity of the BP herbicide released into the aqueous solutions was measured at λ_{max} = 246.4 nm using a Perkin Elmer ultraviolet-visible spectrometer.

3. Results and discussion

3.1. Powder X–ray diffraction analysis

The PXRD patterns of zinc hydroxide nitrate–sodium dodecylsulphate (ZHN–SDS), bispyribac (BP), and zinc hydroxide nitrate–sodium dodecylsulphate–bispyribac (ZHN–SDS–BP) nanocomposites with different BP concentrations (0.02–0.1 M) are displayed in Fig. 2.

Fig. 2(a) presents the PXRD pattern of the ZHN–SDS that was prepared by coprecipitation. The diffraction peak at 2.2°

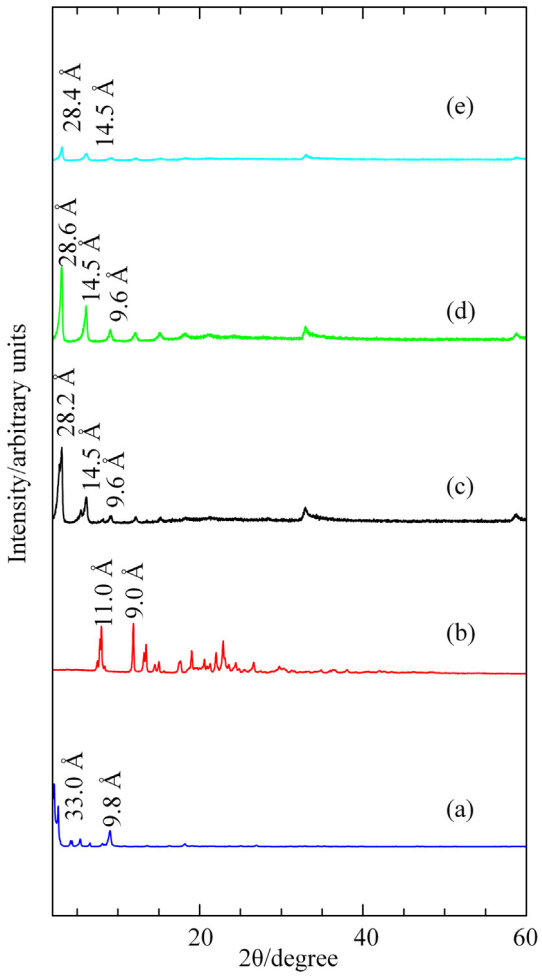

Fig. 2 PXRD Patterns of (a) ZHN–SDS, (b) BP, and ZHN–SDS–BP Prepared using (c) 0.02 M (d) 0.05 M and (e) 0.1 M BP.

corresponds to a basal spacing of 33.0 Å, allowing the SDS to adopt an approximately vertical monolayer arrangement in the interlayer gallery of ZHN (Qiu et al., 2009). The formation of ZHN–SDS layered nanosheet using $Zn(NO_3)_2$, via coprecipitation method is elucidated as:

$$Zn(NO_3)_2 \rightarrow Zn^{2+}\ (aq) + 2(NO_3)^-\ (aq) \quad (1)$$

$$Zn^{2+}\ (aq) + H_2O \rightleftharpoons ZnOH^+\ (aq) + H^+\ (aq) \quad (2)$$

$$Zn(OH)_{2-x}{}^{x+} + x/4O_2 \rightarrow ZnO + (1–1/2x)H_2O \quad (3)$$

$$Zn(OH)_{2-x}{}^{x+} + xDS^- \rightarrow Zn(OH)_{2-x}DSx \quad (4)$$

The solubility of $Zn(NO_3)_2$ in water allowing the zinc species to undergo hydrolysis reaction, as shown in Eqs. (1) and (2) (Moezzi et al., 2013). Even though the zinc hydroxide species produced during the hydrolysis process can be further converted into ZnO, the presence of dodecyl sulphate ions in the reaction, however, permitting the dodecyl sulphate ions to be charge-assembled with the zinc hydroxide species, hence forming the ZHN–SDS layered nanosheet. The related equations were presented as shown in Eqs. (3) and (4) (Liang et al., 2011).

After the intercalation of BP, the basal spacing of ZHN–SDS–BP decreases (Fig. 2(c)–(e)). The diffraction peaks located at 3.1–3.2° correspond to a basal spacing of 28.2–28.6 Å. Although the basal spacing of ZHN–SDS–BP is quite different than that of ZHN–SDS, it is still large enough to occupy both SDS and BP, although the SDS may be tilted slightly, or some of the SDS molecules may have been eliminated from the interlayer gallery to form SDS–BP micelles in the solution (Liu et al., 2015). A similar pattern of basal spacing reduction when intercalating guest ions into surfactant–treated layered materials has been reported in recent studies (Liu et al., 2015; Qiu et al., 2009). The PXRD patterns of the ZHN–SDS–BP nanocomposites exhibit turbostratic disorder, which is denoted by the appearance of saw–toothed peaks located at 33°. The turbostratic effect was induced by both the highly separated layers and the weak interactions between the interlayer species and the host lattice (Li et al., 2008; Rives and Ulibarri, 1999).

The results obtained from the PXRD analyses also reveal that the intercalation trend of the ZHN–SDS–BP was affected by the BP concentration. The PXRD patterns in Fig. 2(c)–(e) show that a new lamellar structure, which is attributed to ZHN–SDS–BP, can be distinctly observed. Although intercalation peaks appear with 0.02 M BP, they are not symmetrical. However, when the BP concentration was increased to 0.05 M, a series of symmetrical, sharp, and intense peaks were displayed, thereby revealing that the nanocomposite is formed of well–ordered layers (Chen et al., 2009). Furthermore, this nanocomposite also possesses better intensity and crystallinity than that with 0.1 M BP. In fact, the intercalated peaks diminished when the ZHN–SDS–BP nanocomposite was synthesised using 0.1 M BP. Hence, the nanocomposite with 0.05 M BP was chosen to be further characterised. The PXRD patterns did not detect any impurities of zinc oxide.

During the intercalation of SDS into the interlayer gallery of ZHN, the three oxygen atoms of the SO_3 group are attracted to the ZHN layer via electrostatic attraction (Liu et al., 2015). The huge basal spacing of ZHN–SDS (33.0 Å) reveals that the SDS sit perpendicularly to the ZHN layer, forming a monolayer arrangement. The intercalation of SDS enlarges the interlayer gallery, thus making it easier for BP to be intercalated (Tao et al., 2009). When BP is introduced, its negatively charged carboxylate group is attracted to the positively charged ZHN layer. This electrostatic attraction enables both SDS and BP to maintain their position in the interlayer gallery of ZHN (Mac Hado et al., 2010). The suggested mechanism for the intercalation is illustrated in Fig. 3.

3.2. Spatial orientation of SDS and BP in the ZHN interlayer

The three–dimensional sizes of BP and SDS molecules were predicted by Chem 3D Ultra 8.0 software and are displayed in Figs. 4 and 5, respectively. It was determined that the x, y, and z axes of BP are 11.6 Å, 16.2 Å, and 10.1 Å, whereas the x, y, and z axes of SDS were determined to be 6.1 Å, 19.9 Å, and 5.2 Å. The height of the interlayer gallery of ZHN–SDS–BP (taken as 28.6 Å from the PXRD analysis) allows prediction of the space available for the intercalation agents. Hence, by deducting the thickness of the hydroxide layer (4.8 Å) and two zinc tetrahedron (2.6 Å × 2), the interlayer space available for the intercalated SDS and BP was cal-

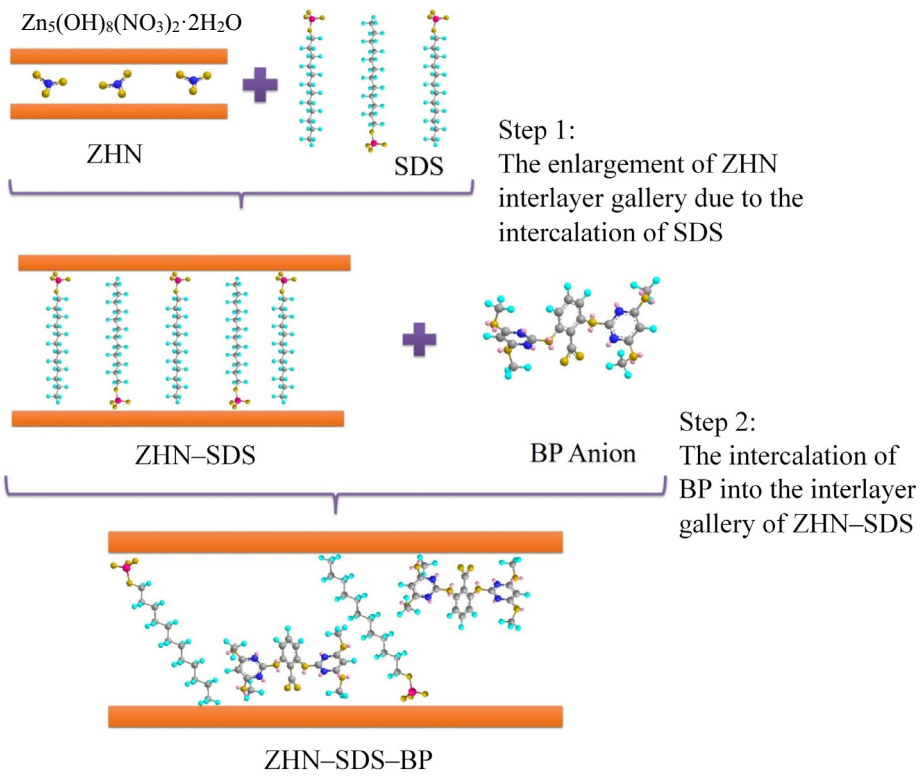

Fig. 3 The Intercalation Mechanism of the ZHN–SDS–BP.

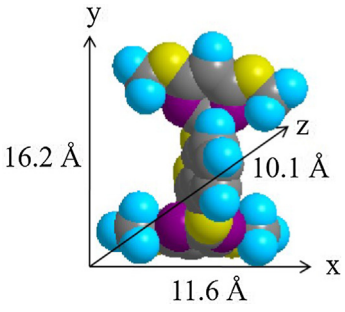

Fig. 4 Three–Dimensional Molecular Structure of BP.

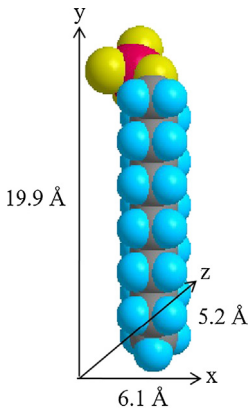

Fig. 5 Three–Dimensional Molecular Structure of SDS.

culated to be 18.6 Å. As the longest axis of the SDS molecule is 19.9 Å, the SDS molecules are believed to sit in a tilted monolayer arrangement in the interlayer gallery (Liu et al., 2015). The predicted spatial orientation of SDS and BP in the interlayer gallery of ZHN is shown in Fig. 6.

3.3. Fourier transform infrared analysis

FTIR analyses were conducted on ZHN–SDS, BP, and ZHN–SDS–BP to validate the presence of SDS and BP in the interlayer gallery of the host, and the FTIR spectra obtained is illustrated in Fig. 7.

The FTIR spectra of ZHN–SDS and ZHN–SDS–BP show a broad peak that represents the stretching vibration of the —OH groups of interlayer water molecule appeared at 3458 cm^{-1} and 3460 cm^{-1} (Al-Kahtani and Sherigara, 2014). A sharp peak that corresponds to the well–defined vibrational energy of —OH in the organic lattice was also present, at 3575 cm^{-1} (Liu et al., 2015). Several characteristic peaks of SDS can be seen in the FTIR spectra of both ZHN–SDS and ZHN–SDS–BP. In the FTIR spectra of ZHN–SDS, the symmetric peak is at 1085 cm^{-1} and the asymmetric peak is at 1217 cm^{-1}. The peak that corresponding to the stretching vibration of S—O emerged at 827 cm^{-1} (Liu et al., 2015; Qiu et al., 2009). Comparable peaks were also observed in the FTIR spectra of ZHN–SDS–BP, at 1178 and 948 cm^{-1}, which represent symmetric peak and asymmetric peak of S═O, respectively, and at 776 cm^{-1} which represent S—O stretching, respectively. These results therefore validate the presence of

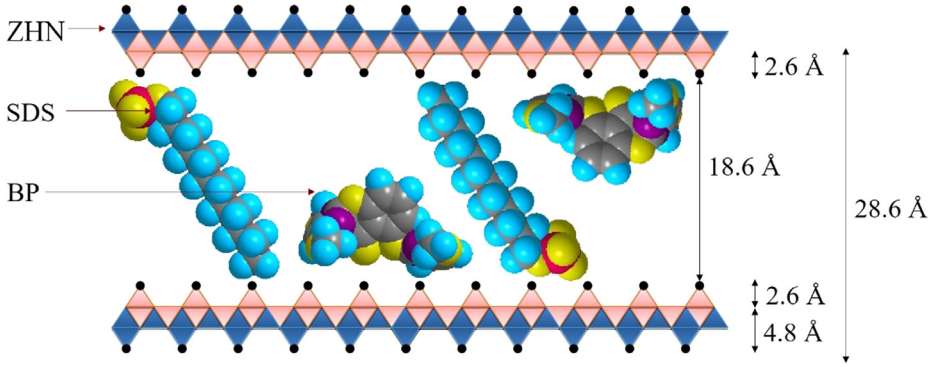

Fig. 6 Spatial Orientation of BP and SDS in the Interlayer Gallery of ZHN–SDS–BP.

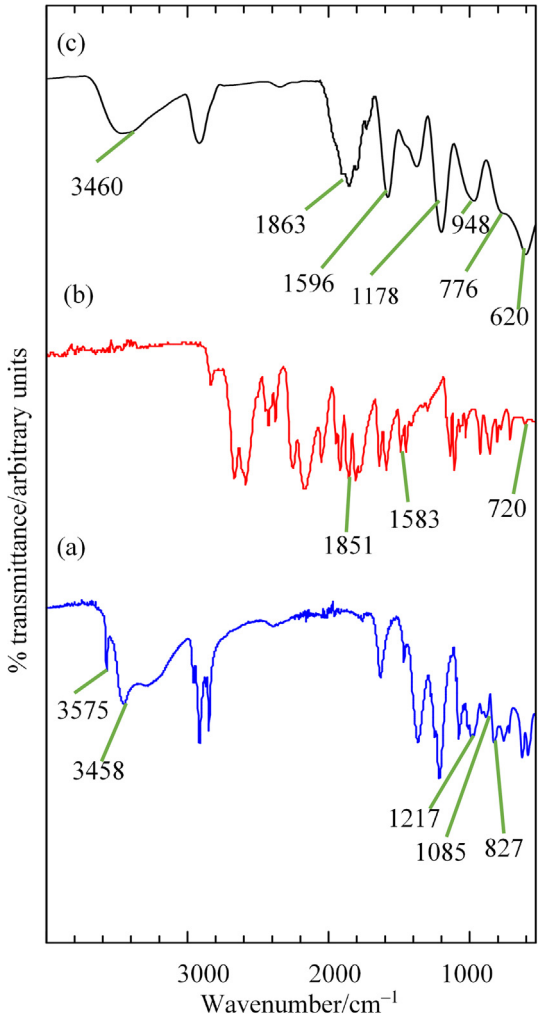

Fig. 7 FTIR Spectra of (a) ZHN–SDS, (b) BP and (c) ZHN–SDS–BP.

SDS in the interlayer galleries of ZHN–SDS and ZHN–SDS–BP.

The FTIR analysis also reveals several similar peaks in the FTIR spectra of BP and ZHN–SDS–BP. Peaks corresponding to the aromatic overtones of ring bonds appeared in the FTIR spectra of BP and ZHN–SDS–BP at 1851 and 1863 cm^{-1}, respectively (Woranuch and Yoksan, 2013). In the FTIR spectra of BP, a peak emerged at 1596 cm^{-1} which represents the C═C stretching of aromatic compounds, and another appeared at 620 cm^{-1} that corresponds to the C—H vibration of benzene rings (Hashim et al., 2014). These peaks are comparable with those at 1587 and 720 cm^{-1} in the FTIR spectra of ZHN–SDS–BP. The characteristic BP peaks in the FTIR spectra of ZHN–SDS–BP therefore confirm that BP is present in the interlayer gallery, along with SDS molecules.

3.4. Thermal stability studies

The TGA/DTG curves for ZHN–SDS, BP, and ZHN–SDS–BP were examined and are shown in Fig. 8. In the TGA/DTG curve of ZHN–SDS (Fig. 8(a)), two thermal decomposition peaks were observed: the first thermal decomposition, with 3.2% weight loss, occurred at 107.1 °C due to the elimination of water molecules present on the surface and in the interlayer gallery of ZHN–SDS; and a major weight loss (of 37.2%) was observed at 198.2 °C, resulting from the decomposition and the combustion of SDS (Liu et al., 2015; Tao et al., 2009). Pristine BP demonstrated thermal decompositions in two separate stages: the first was at 313.0 °C, with an abrupt weight loss of 46.3%; and the second was at 512.5 °C, with 26.4% weight loss. These stages are due to decomposition related to decarboxylation and deamination (Shulman and Simmonds, 1968).

The thermal decomposition of ZHN–SDS–BP happened in three stages. The first thermal decomposition, with minor weight loss (of 5.4%), occurred at 91.7 °C due to water molecule removal. The second thermal decomposition occurred at 203.0 °C, with major weight loss (of 34.8%), owing to the combustion of the SDS. The final thermal decomposition, at 576.0 °C with weight loss of 13.7%, resulted from the decomposition of the organic moiety originated from the intercalated BP (Liu et al., 2015). The maximum decomposition temperature of the ZHN–SDS–BP nanocomposite (576.0 °C) is higher than that of pristine BP (512.5 °C), showing that the intercalation of BP into the interlayer gallery of ZHN–SDS could improve the thermal stability of BP.

3.5. Elemental analysis

The chemical compositions of ZHN–SDS, BP, and ZHN–SDS–BP, as determined by ICP–OES and CHNS analyses,

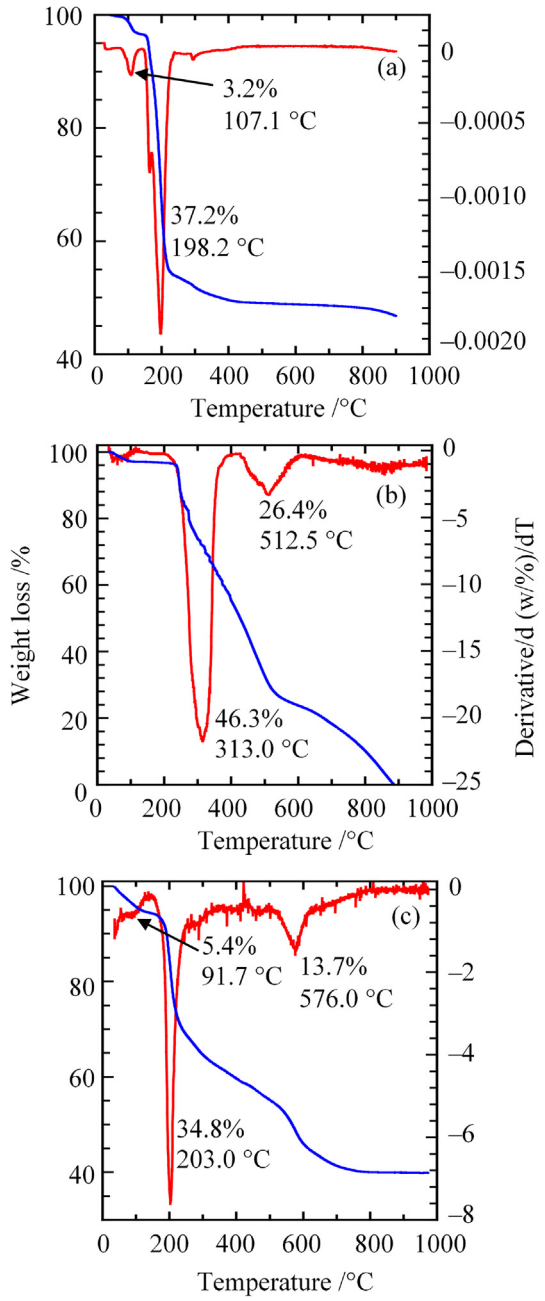

Fig. 8 TGA/DTG Curves of (a) ZHN–SDS, (b) BP and (c) ZHN–SDS–BP.

are tabulated in Table 1. The percentage loading of BP in the interlayer of ZHN–SDS–BP (61.34%) was calculated from the percentage of nitrogen (8.00%) The elemental analysis therefore supports the success of BP intercalation into the interlayer gallery of ZHN–SDS.

3.6. Surface morphology analysis

FESEM images of ZHN–SDS and ZHN–SDS–BP are shown in Fig. 9(a) and (b), respectively. Although they show that the morphology of ZHN–SDS and ZHN–SDS–BP are slightly different, both nanocomposites maintain a resemblance to a thin lamellar flake–like sheet structure, as expected for layered materials (Arizaga et al., 2007). ZHN–SDS shows a tabular and non–porous structure with sharp edges, whereas ZHN–SDS–BP shows a non–porous structure with more rounded edges. The intercalation of BP into ZHN–SDS therefore slightly changes the morphology of the host.

3.7. Surface properties analysis

The nitrogen adsorption–desorption isotherms of ZHN–SDS and ZHN–SDS–BP are shown in Fig. 10. The curves reveal that both isotherms are of Type IV (according to IUPAC classification), which signifies the adsorption has a mesoporous nature with a hysteresis loop (Sing, 1985). The nitrogen uptake for both ZHN–SDS and ZHN–SDS–BP occurred very slowly at low relative pressures; however, it increased rapidly at relative pressures above 0.55 for ZHN–SDS and 0.4 for ZHN–SDS–BP. This rapid adsorption continued until the optimum adsorption was achieved (32 and 11 $cm^3\ g^{-1}$ for ZHN–SDS and ZHN–SDS–BP, respectively). The desorption branch of the hysteresis loop seems to be slightly wider for ZHN–SDS–BP than for ZHN–SDS, which indicates that the materials have a different pore texture (Sarijo et al., 2015).

The Barrett–Joyner–Halenda (BJH) desorption pore size distribution curves for ZHN–SDS and ZHN–SDS–BP are illustrated in Fig. 11. Two intense peaks can be observed at around 1.4 nm and 7.6 nm for ZHN–SDS, whereas five sharp peaks centred around 1.4 nm, 1.8 nm, 2.4 nm, 3.8 nm, and 4.8 nm can be observed for ZHN–SDS–BP. The BJH average pore diameters for ZHN–SDS and ZHN–SDS–BP were determined to be 27.83 nm and 31.48 nm, respectively. The data obtained shows that the Brunauer–Emmett–Teller (BET) surface area of ZHN–SDS decreased from 7.03 $m^2\ g^{-1}$ to 2.12 $m^2\ g^{-1}$ after the BP intercalation. A reduction in the total pore volume was also observed, from 0.05 $cm^3\ g^{-1}$ in ZHN–SDS to 0.02 $cm^3\ g^{-1}$ in ZHN–SDS–BP. It is suggested that the decrease in surface area and pore volume is due to pore blockage that occurs after intercalation (Hamada et al., 2007).

A summary of the surface properties is provided in Table 2. Hence, the results prove that intercalation of BP alters the surface properties of ZHN–SDS, in terms of surface area and porosity.

Table 1 Elemental Chemical Composition of ZHN–SDS, BP and ZHN–SDS–BP.

Sample	Zn (%)	C (%)	H (%)	N (%)	S (%)	[a]BP (%w/w)	
ZHN–SDS	24.14	24.80	5.48	2.46	3.38	–	
BP	–	47.33	3.83	10.28	–	–	$C_{19}H_{17}N_4O_8$
ZHN–SDS–BP	37.57	32.71	2.94	8.00	0.01	61.34	

[a] = estimated from the percentage of nitrogen obtained from CHNS analysis.

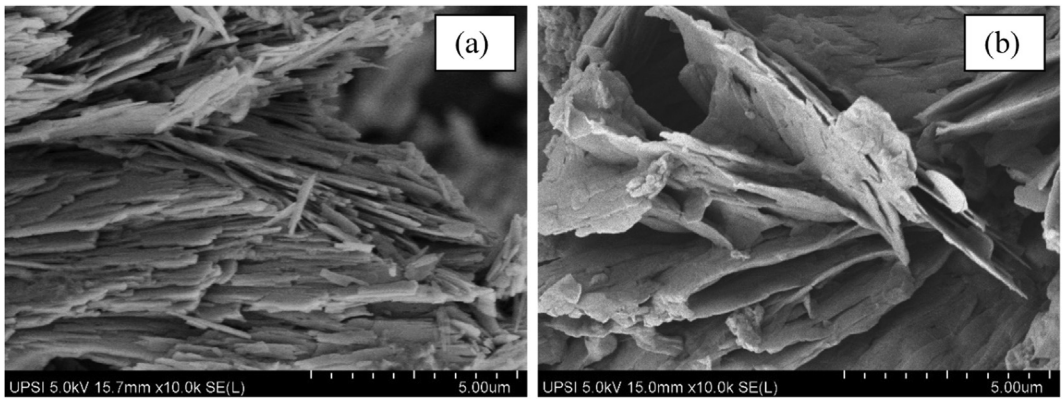

Fig. 9 Surface Morphology of (a) ZHN–SDS and (b) ZHN–SDS–BP.

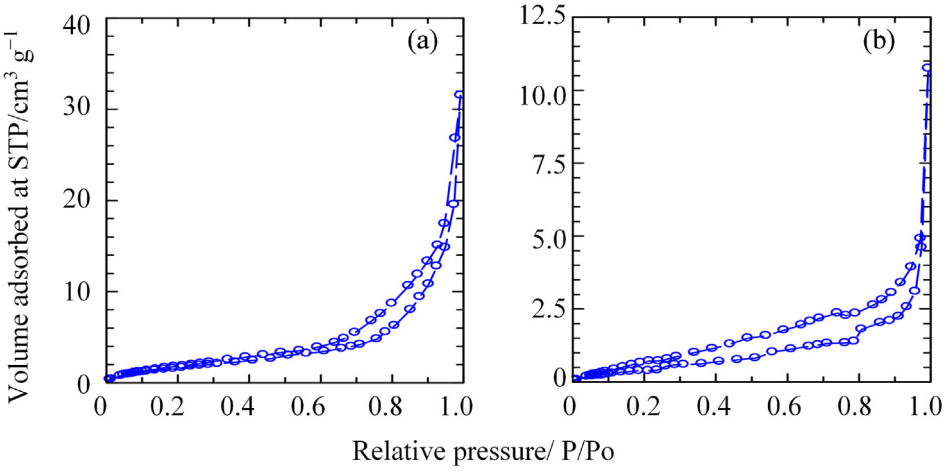

Fig. 10 Adsorption–Desorption Isotherms of Nitrogen Gas for (a) ZHN–SDS and (b) ZHN–SDS–BP.

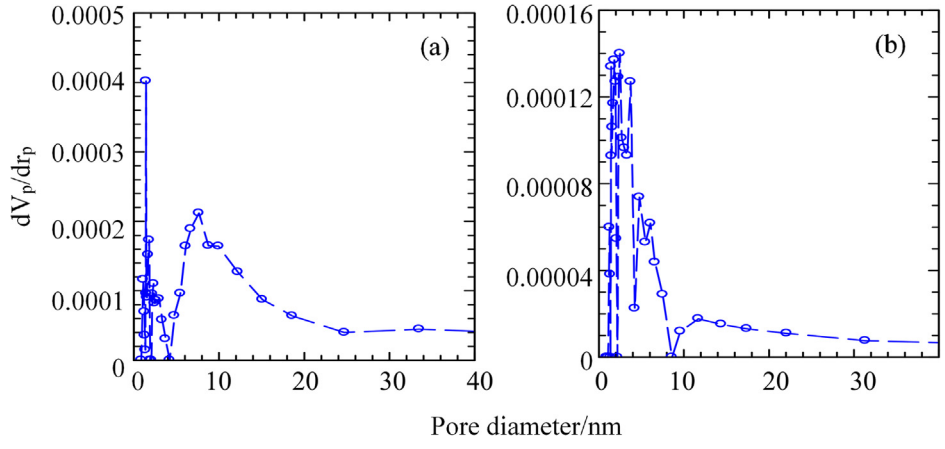

Fig. 11 BJH Desorption Pore Size Distributions for (a) ZHN–SDS and (b) ZHN–SDS–BP.

3.8. Release study of BP from ZHN–SDS–BP into single, binary and ternary system of aqueous solutions

Owing to the fact that BP is a type of herbicide that is usually used to control common barnyard grass and numerous floating, submersed and emergent weeds found in paddy cultivation areas, aqueous solutions containing PO_4^{3-}, SO_4^{2-} and Cl^- were also selected as the release media to simulate the actual soil environment of the paddy cultivation. The release profiles corresponding to the release of intercalated BP into different concentrations and anion compositions of aqueous solutions were plotted against time and are demonstrated in Fig. 12.

Table 2 Surface Properties of ZHN–SDS and ZHN–SDS–BP.

Sample	Basal spacing (Å)	Total pore volume ($cm^3\ g^{-1}$)	Multipoint BET surface area ($m^2\ g^{-1}$)	BJH average pore diameter (nm)
ZHN–SDS	33.0	0.049	7.027	27.830
ZHN–SDS–BP	28.6	0.017	2.117	31.480

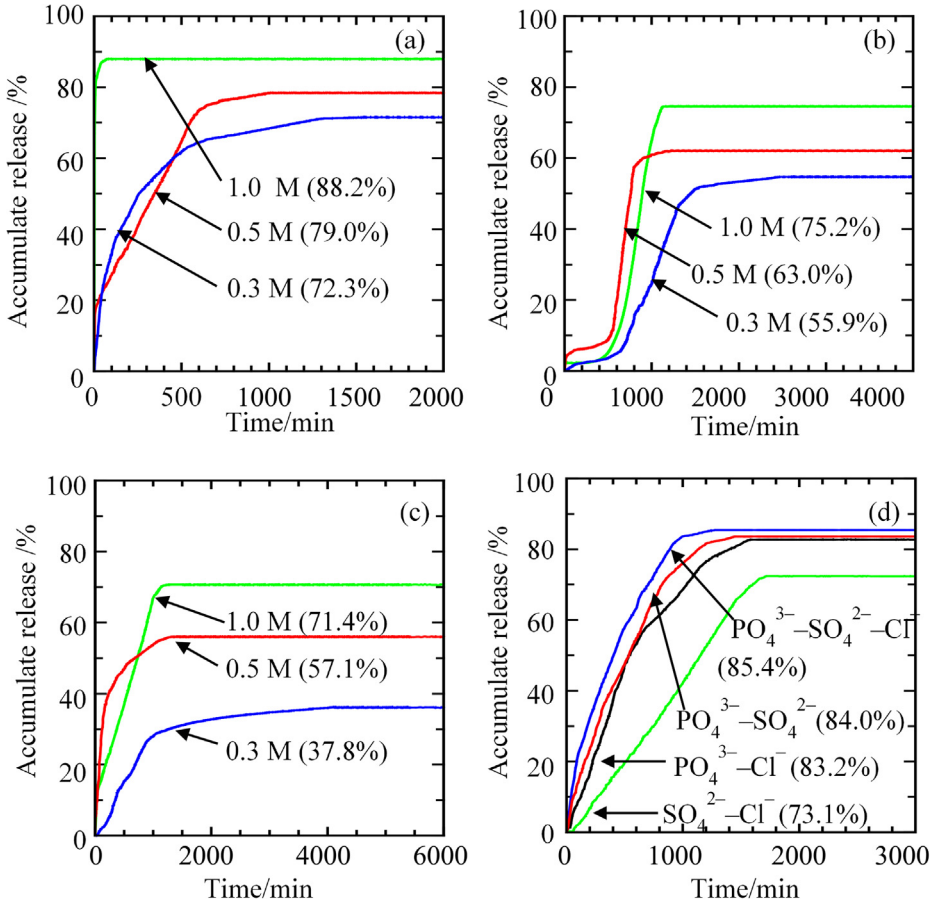

Fig. 12 Release Profiles of BP from ZHN–SDS–BP into Aqueous Solutions of (a) Sodium Phosphate, (b) Sodium Sulphate, (c) Sodium Chloride and (d) Phosphate, Sulphate and Chloride Mixture.

The release profiles reveal that significant differences in the percentage releases were obtained when varying the type and concentration of the aqueous solutions. In the single system of aqueous solution, the maximum percentage release obtained when BP was released from the ZHN–SDS–BP nanocomposite in the 1.0 M aqueous solution of Na_3PO_4 was 88.2%. Lower percentage releases were observed when aqueous solutions of Na_2SO_4 (1.0 M) and NaCl (1.0 M) were used as the release media, with 75.2% and 71.4%, respectively. This observation indicates that the percentage release of BP from the interlayer gallery of the ZHN–SDS–BP nanocomposite decreases in the order of Na_3PO_4 > Na_2SO_4, > NaCl. The greater affinity possessed by the trivalent PO_4^{3-} compared to SO_4^{2-} and Cl^- makes the PO_4^{3-} more attracted towards the positively charged layer of ZHN, hence making it is easier for the PO_4^{3-} to replace the intercalated BP. Reducing the concentration of the aqueous solutions was found to slightly lower the resulting percentage release. The percentage releases in Na_3PO_4 were observed to decrease to 79.0% (0.5 M) and 72.3% (0.3 M), the percentage releases in Na_2SO_4 decreased to 63.0% (0.5 M) and 55.9% (0.3 M), whereas the percentage releases in NaCl decreased to 57.1% (0.5 M) and 37.8% (0.3 M). This reduction thereby shows that the lower amount of anions that were initially present in the aqueous solutions of lower concentration favours less BP to be released into the aqueous solutions, hence lowering their maximum percentage release. These findings also revealed that the release of BP in all aqueous solutions is concentration dependent.

The justification of the release processes according to their release times demonstrates that the maximum percentage release of BP from the interlayer gallery of ZHN–SDS–BP in the aqueous solutions of 0.3 M, 0.5 M and 1.0 M of Na_3PO_4 were achieved in 1535 min, 1010 min and 74 min, respectively. The release process in the aqueous solutions of Na_3PO_4 gener-

ally started with faster release in the beginning part of the release process, followed by slower release. As for the release of BP from the interlayer gallery of ZHN–SDS–BP into the aqueous solutions of 0.3 M, 0.5 M and 1.0 M of Na_2SO_4, the times needed for the release process to reach maximum percentage release are 2435 min, 1224 min, and 1125 min, respectively, which are obviously longer compared to the release process in the aqueous solutions of Na_3PO_4. The pattern of the release process was also found to be marginally different compared to the release process in the aqueous solutions of Na_3PO_4. The release process occurred slowly at the beginning of the release process, followed by a faster release process that was subsequently followed by slower release before reaching the maximum percentage release. This release trend is explained by the fact that the divalent SO_4^{2-} presence in the aqueous solution of Na_2SO_4 has lower charge density and less affinity towards the ZHN layer compared to the trivalent PO_4^{3-}, hence slowing the release process.

The times needed for the ZHN–SDS–BP nanocomposite to release the intercalated BP to reach maximum percentage

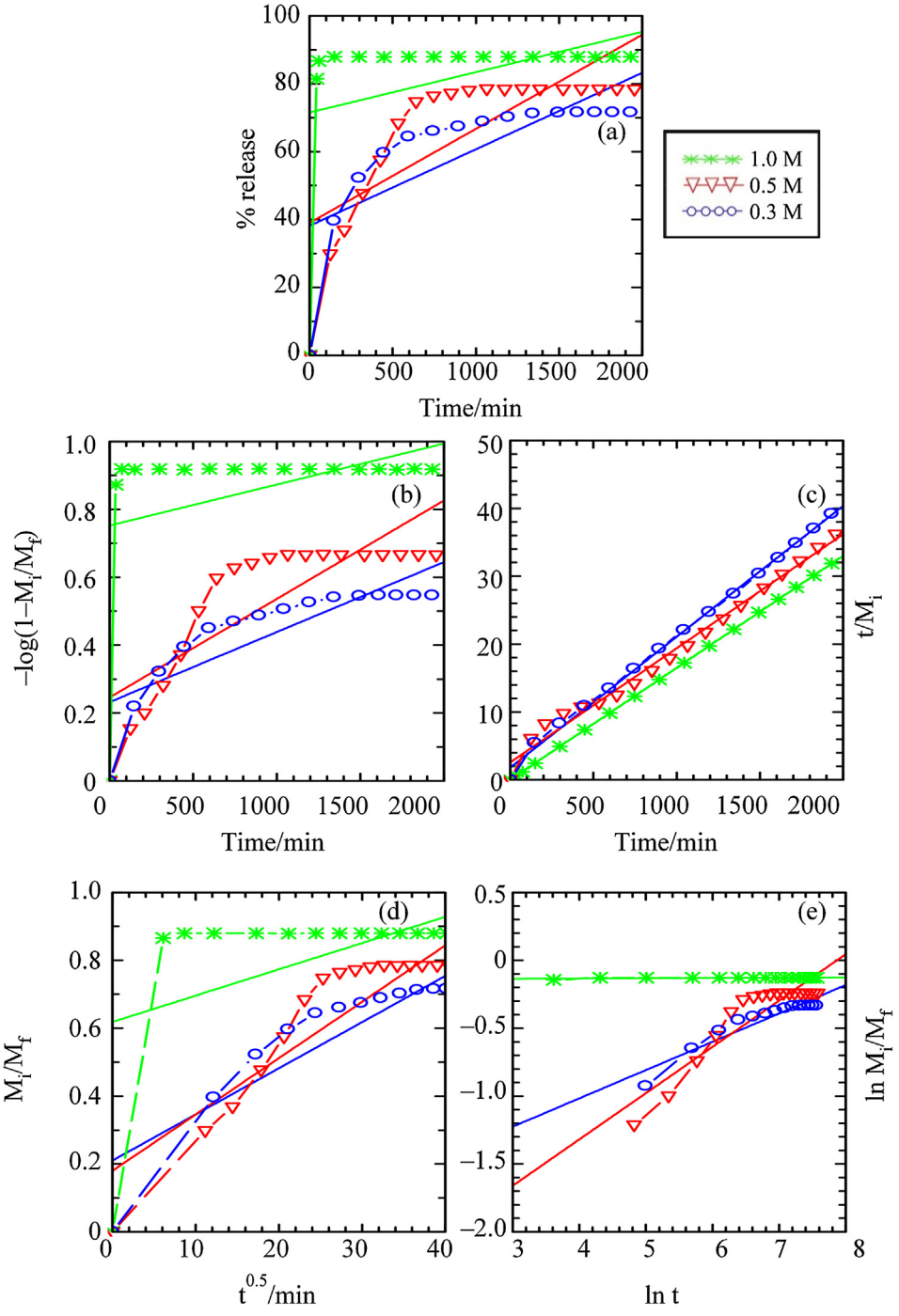

Fig. 13 Fitting of the Data for BP Release from ZHN–SDS–BP into Aqueous Solution of Sodium Phosphate for the (a) Zero Order, (b) First Order, (c) Pseudo Second Order, (d) Parabolic Diffusion and (e) Fickian Diffusion Kinetic Models.

release in the aqueous solutions of 0.3 M, 0.5 M and 1.0 M NaCl are 4117 min, 1326 min, and 1230 min. The slowest release process that occurred when aqueous solutions of NaCl were used as the release media is due to the fact that the Cl^- is a monovalent anion with a lower charge density compare to PO_4^{3-} and SO_4^{2-}. Unlike the release process in the aqueous solutions of Na_2SO_4, the release process of BP from the ZHN–SDS–BP nanocomposite began with a faster release at the beginning of the release process, followed by a slower release process. Although the Cl^- has less charge density and a lower affinity towards the positively charged ZHN layer than SO_4^{2-}, the fact that Cl^- exists as a monoatomic ion, whereas SO_4^{2-} exists as a polyatomic ion, plays a significant role in making the ion exchange process between the Cl^- and the intercalated BP easier, hence increasing the rate of release of the intercalated BP in the early part of the release process. Comparing the results obtained in terms of the time release for the release process also reveals that the increasing concentration of the aqueous solution accelerates the release process. More anions provided by a higher concentration of aqueous solution act as a driving force to quicken the release process. Hence, signifying that the release process is concentration dependent.

As for the release of BP from the interlayer gallery of the ZHN-SDS-BP nanocomposite in binary and ternary aqueous

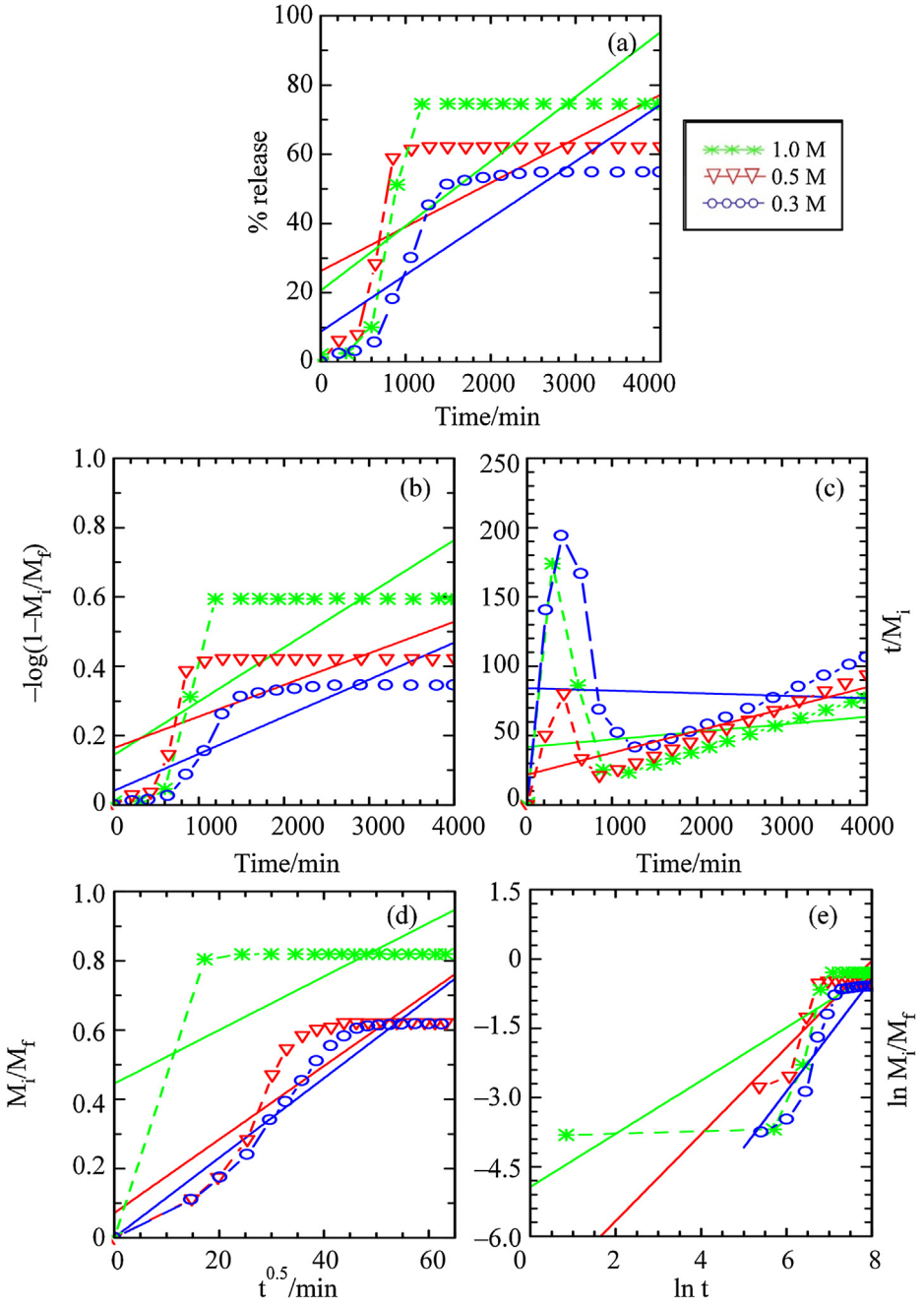

Fig. 14 Fitting of the Data for BP Release from ZHN–SDS–BP into Aqueous Solution of Sodium Sulphate for the (a) Zero Order, (b) First Order, (c) Pseudo Second Order, (d) Parabolic Diffusion and (e) Fickian Diffusion Kinetic Models.

systems, the release study was investigated using aqueous solutions of PO_4^{3-}–SO_4^{2-}, PO_4^{3-}–Cl^-, SO_4^{2-}–Cl^- and PO_4^{3-}–SO_4^{2-}–Cl^- as the release medium. Different pattern of release profile obtained when varying the composition of anions in the release medium demonstrate that different anion combination will trigger different release behaviour of the BP. The justification of the release behaviour were made based on the percentage of the accumulated release, and can be arranged as; PO_4^{3-}–SO_4^{2-}–Cl^- > PO_4^{3-}–SO_4^{2-} > PO_4^{3-}–Cl^- > SO_4^{2-}–Cl^-. The release profile show that 85.4% of intercalated BP were release in the aqueous solution of PO_4^{3-}–SO_4^{2-}–Cl^- within 1271 min, 84.0% were released in the aqueous solution of PO_4^{3-}–SO_4^{2-} within 1318 min, whereas 83.2% and 73.1% of BP were released in the aqueous solutions of PO_4^{3-}–Cl^- and SO_4^{2-}–Cl^- within 1425 min and 1611 min, respectively. The aqueous solutions with PO_4^{3-} anion as one of their component were revealed to have higher percentage of accumulated release. This findings can be explained based on the higher affinity possess by the PO_4^{3-} anion compare the SO_4^{2-} and Cl^-, which makes the PO_4^{3-} anion to have stronger attraction toward the positively charged ZHN-SDS host (Sarijo et al., 2015). The reduction of percentage release in the aqueous solution containing Cl^-

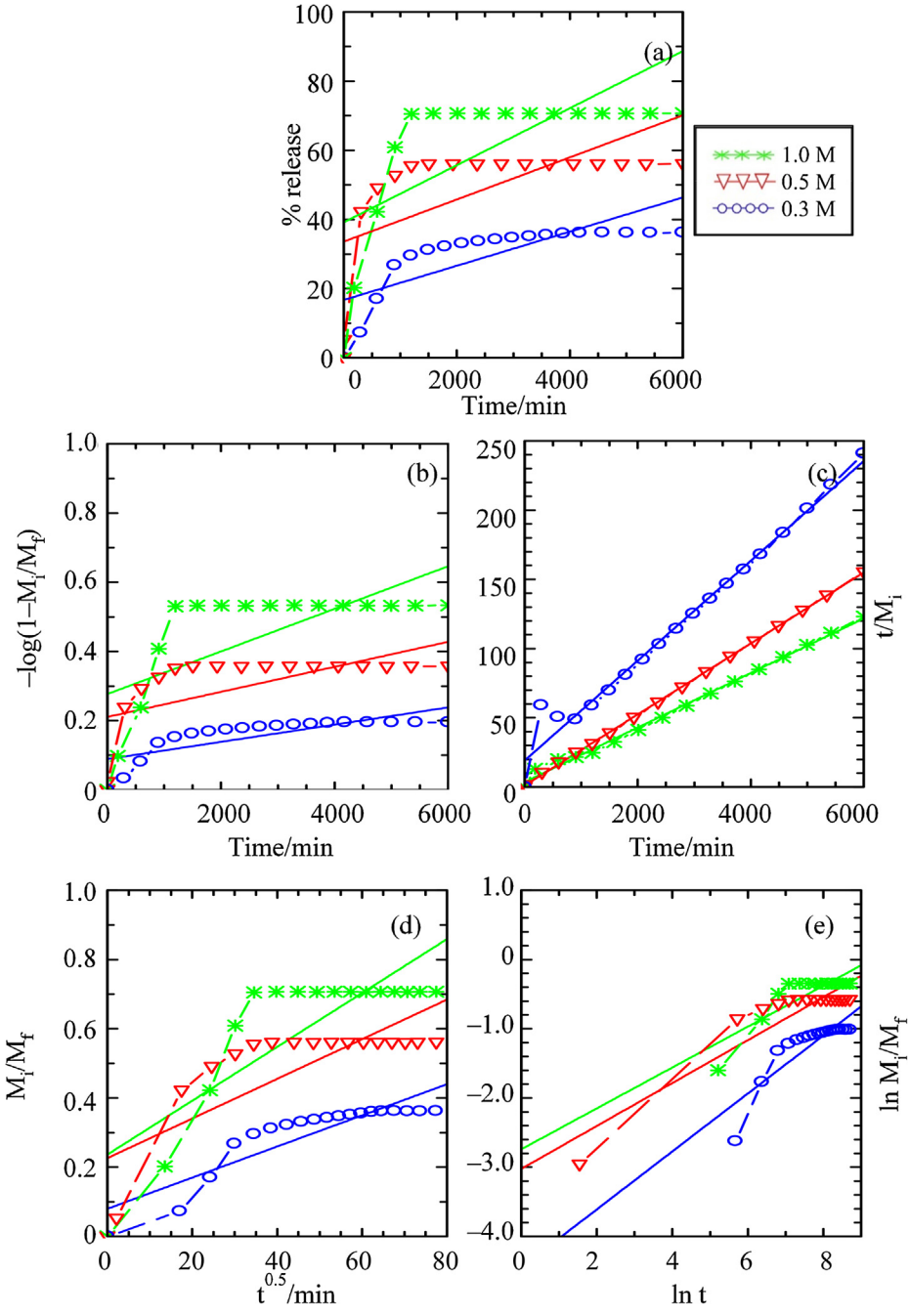

Fig. 15 Fitting of the Data for BP Release from ZHN–SDS–BP into Aqueous Solution of Sodium Chloride for the (a) Zero Order, (b) First Order, (c) Pseudo Second Order, (d) Parabolic Diffusion and (e) Fickian Diffusion Kinetic Models.

Table 3 Comparison of Rate Constants (k), Regression Values (r^2) and Half–Life ($t_{1/2}$) Obtained from the Fitting of the Release Data from ZHN–SDS–BP into Aqueous Solutions of Na_3PO_4, Na_2SO_4 and NaCl.

Aqueous Solution		Zero order	First order	Parabolic diffusion	Fickian diffusion	Pseudo second order		
		r^2	r^2	r^2	r^2	r^2	k ($\times 10^{-3}$ s^{-1})	$t_{1/2}$
Na_3PO_4	0.3 M	0.553	0.701	0.802	0.896	0.998	0.129	112.5
	0.5 M	0.589	0.683	0.815	0.844	0.988	0.062	235.7
	1.0 M	0.142	0.133	0.255	0.388	1.00	4.267	3.4
Aqueous Solution		Zero order	First order	Pseudo second order	Fickian diffusion	Parabolic diffusion		
		r^2	r^2	r^2	r^2	r^2	k (s^{-1})	$t_{1/2}$
Na_2SO_4	0.3 M	0.735	0.760	0.002	0.841	0.921	0.016	1037.2
	0.5 M	0.497	0.510	0.583	0.773	0.802	0.019	657.9
	1.0 M	0.626	0.643	0.032	0.704	0.786	0.017	835.9
Aqueous Solution		Zero order	First order	Parabolic diffusion	Fickian diffusion	Pseudo second order		
		r^2	r^2	r^2	r^2	r^2	k ($\times 10^{-3}$ s^{-1})	$t_{1/2}$
NaCl	0.3 M	0.597	0.605	0.795	0.747	0.981	0.022	668.7
	0.5 M	0.366	0.382	0.607	0.847	1.000	0.120	120.7
	1.0 M	0.450	0.467	0.673	0.396	0.996	0.030	483.0

indicate that the release of BP was affected by the monovalent nature of Cl-, which has less affinity toward the ZHN-SDS layer.

3.9. Kinetic study of ZHN–SDS–BP into various aqueous solutions

The release of guest ions intercalated in the host material into the release media may involve various process, such as ion exchange process, diffusion, erosion and dissolution (Cao et al., 2008; Ghori and Conway, 2015; Li et al., 2008; Lucinda-Silva et al., 2010). Therefore, with the aim of obtaining some insight into the mechanism that controls the release of BP from the ZHN–SDS–BP nanocomposite into various aqueous solutions, the release data were fitted into several kinetic models. The kinetic models selected for this study are zero order, first order, pseudo second order, parabolic diffusion and Fickian diffusion models.

The fitting of the release data into above mentioned kinetic models, performed in the single, binary and ternary systems of Na_3PO_4, Na_2SO_4 and NaCl aqueous solutions, are plotted and shown in Figs. 13–15, respectively. The comparison of the r^2, k and the $t_{1/2}$ values obtained from the data fitting are summarised in Table 3.

The kinetic data presented in Figs. 13–15 and Table 3 show that the release mechanism of BP changes when the releases were performed in different types of aqueous solution. A good linearity ($0.988 \leq r^2 \leq 1.00$) was obtained when the release data of the release study performed in the aqueous solutions of Na_3PO_4 were fitted into a pseudo second order kinetic model. Fitting the data release into other kinetic models shows poorer linearity, with $r^2 \leq 0.896$. The release process governed by the pseudo second order kinetic model indicates that the BP was released from the interlayer gallery of the ZHN–SDS–BP nanocomposite through the dissolution of the nanocomposite and the ion exchange process that occurred between the intercalated BP and the PO_4^{3-}.

As for the release process in the aqueous solution of Na_2SO_4, it can be seen that the parabolic diffusion kinetic model shows better performance in describing the release behaviour, with $0.786 \leq r^2 \leq 0.921$. The release process that was controlled by the parabolic diffusion kinetic model generally describes that the release process was governed by the intraparticle diffusion or surface diffusion, hence signifying that the external surface diffusion or the intraparticle diffusion via ion–exchange is the rate–determining step in the release process (Céspedes et al., 2007). This kinetic model also indicates that the release is proportional to the square root of time (Baker, 1987).

In the case of the release process of BP using aqueous solutions of NaCl as the release media, it can be deduced that the pseudo second order kinetic model is better fitted than the other kinetic model ($0.981 \leq r^2 \leq 1.000$). Therefore, indicating the mechanism of the release process in aqueous solution of NaCl is similar as in the release process when the aqueous solution of Na_3PO_4 is used as the release media, which happened via the dissolution of the ZHN–SDS–BP nanocomposite and the ion exchange between the intercalated BP and the SO_4^{2-}.

4. Conclusion

The intercalation of BP into the interlayer gallery of ZHN has been succeeded with the aid of SDS surfactant. The presence of SDS molecules in the interlayer gallery enlarges the basal spacing of ZHN, hence it is easier for BP to be inserted. The emergence of symmetrical, sharp and intense intercalation peaks at lower 2θ, with a basal spacing of 28.2–28.6 Å, confirmed the intercalation of both SDS and BP, and reveals that the nanocomposite is formed of well-ordered layers. This was further supported by the characterisation study that involved FTIR, ICP-OES, and CHNS analyses. Analysis on the surface morphology and properties demonstrated that the intercalation of BP into the interlayer gallery of ZHN–SDS leads to a

significant change in surface area, porosity, and morphology. The results from the CRF study revealed that the intercalation of BP into the interlayer gallery of ZHN was found to be an efficient way in slowing the release of BP into the aqueous solutions. The release profile in both aqueous solutions of Na_3PO_4 and NaCl presented a pseudo second order kinetic model, thus indicating that the intercalated BP was released into the aqueous solutions via the dissolution of the ZHN-SDS-BP nanocomposite and the ion exchange process between BP and the anions in the aqueous solutions. The released of BP in the aqueous solution of Na_2SO_4 was governed by the parabolic diffusion kinetic model which describes the release through intraparticle and surface diffusion. Therefore, it can be proposed that ZHN is a promising host material in implementing the slow release of BP herbicide for the paddy cultivation sector.

Declaration of Competing Interest

None declared.

Acknowledgments

The authors wish to thank UPSI and the Ministry of Education Malaysia for supporting this research. This work was supported by the GPU-RISING STAR Grant No. 2019–0119–103–01.

Data availability

The raw/processed data required to reproduce these findings cannot be shared at this time due to legal or ethical reasons.

References

Ahmad, F., Anwar, S., Firdous, S., Da-Chuan, Y., Iqbal, S., 2018. Biodegradation of bispyribac sodium by a novel bacterial consortium BDAM: optimization of degradation conditions using response surface methodology. J. Hazard. Mater. 349, 272–281.

Ahmad, F., Ashraf, N., Zhou, R. Bin, Da-Chuan, Y., 2019. Enhanced remediation of bispyribac sodium by wheat (Triticum aestivum)and a bispyribac sodium degrading bacterial consortium (BDAM). J. Environ. Manage. 244, 383–390.

Al-Kahtani, A.A., Sherigara, B.S., 2014. Controlled release of diclofenac sodium through acrylamide grafted hydroxyethyl cellulose and sodium alginate. Carbohydr. Polym. 104, 151–157.

Almalike, L.B., Al-najar, A.A., Kadhim, Z.N., 2015. Adsorption and desorption characteristics of bispyribac-sodium pesticide in eight soil in south of Iraq 6, 1689–1700.

Arizaga, G.G.C., Mangrich, A.S., da Costa Gardolinski, J.E.F., Wypych, F., 2008. Chemical modification of zinc hydroxide nitrate and Zn-Al-layered double hydroxide with dicarboxylic acids. J. Colloid Interface Sci. 320, 168–176.

Arizaga, G.G.C., Satyanarayana, K.G., Wypych, F., 2007. Layered hydroxide salts: synthesis, properties and potential applications. Solid State Ionics 178, 1143–1162.

Baker, R., 1987. Controlled Release of Biologically Active Agents. John Wiley & Sons, New York.

Bravo-Suárez, J.J., Páez-Mozo, E.A., Oyama, S.T., 2004. Review of the synthesis of layered double hydroxides: a thermodynamic approach. Quim. Nova 27, 601–614.

Bruna, F., Celis, R., Pavlovic, I., Barriga, C., Cornejo, J., Ulibarri, M. A., 2009. Layered double hydroxides as adsorbents and carriers of the herbicide (4-chloro-2-methylphenoxy)acetic acid (MCPA): systems Mg-Al, Mg-Fe and Mg-Al-Fe. J. Hazard. Mater. 168, 1476–1481.

Cao, G.T., Xing, F.F., Wang, P., Ni, Z.M., 2008. Synthesis, characterization and release of curcumin-intercalated Mg-Al-layered double hydroxides. Chinese J. Inorg. Chem. 24, 956–963.

Céspedes, F.F., Sánchez, M.V., García, S.P., Pérez, M.F., 2007. Modifying sorbents in controlled release formulations to prevent herbicides pollution. Chemosphere 69, 785–794.

Chauhan, B.S., Johnson, D.E., 2010. The role of seed ecology in improving weed management strategies in the tropics. Adv. Agron. 105, 221–262.

Chen, Q., Shi, S., Liu, X., Jin, L., Wei, M., 2009. Studies on the oxidation reaction of l-cysteine in a confined matrix of layered double hydroxides. Chem. Eng. J. 153, 175–182.

Cordeiro, C.S., Arizaga, G.G.C., Ramos, L.P., Wypych, F., 2008. A new zinc hydroxide nitrate heterogeneous catalyst for the esterification of free fatty acids and the transesterification of vegetable oils. Catal. Commun. 9, 2140–2143.

Cristina, A., Cursino, T., Lisboa, S., Pyrrho, S., Pereira, V., Sousa, D., Wypych, F., 2013. Layered double hydroxides intercalated with anionic surfactants/benzophenone as potential materials for sunscreens. J. Colloid Interface Sci. 397, 88–95.

Durborow, R.M., 2014. Management of aquatic weeds. In: Chauhan, B.S., Mahajan, G. (Eds.), Recent Advances in Weed Management. Springer, New York, pp. 281–314.

Fernandes, F.M., Baradari, H., Sanchez, C., 2014. Integrative strategies to hybrid lamellar compounds: an integration challenge. Appl. Clay Sci. 100, 2–21.

Galla, M.F., Hanson, B.D., Al-Khatib, K., 2019. Detection of bispyribac-sodium residues in walnut leaves after simulated drift. Horttechnology 29, 25–29.

Ghori, M.U., Conway, B.R., 2015. Hydrophilic matrices for oral control drug delivery. Am. J. Pharmacol. Sci. 3, 103–109.

Hamada, S., Hibarino, S., Ikeue, K., Machida, M., 2007. Preparation of supported Pt-M catalysts (M = Mo and W) from anion-exchanged hydrotalcites and their catalytic activity for low temperature $NO-H_2-O_2$ reaction. Appl. Catal. B Environ. 74, 197–202.

Hashim, N., Hussein, M.Z., Isa, I., Kamari, A., Mohamed, A., Jaafar, A.M., Taha, H., 2014. Synthesis and controlled release of cloprop herbicides from cloprop-layered double hydroxide and cloprop-zinc-layered hydroxide nanocomposites. Open J. Inorg. Chem. 4, 1–9.

He, J., Wei, M., Li, B., Kang, Y., Evans, D.G., Duan, X., 2006. Preparation of layered double hydroxides. In: Layered Double Hydroxides. Springer Berlin Heidelberg, New York, pp. 89–119.

Hong, J., Zhu, Z., Lu, H., Qiu, Y., 2014. Synthesis and arsenic adsorption performances of ferric-based layered double hydroxide with α-alanine intercalation. Chem. Eng. J. 252, 267–274.

Hussein, M.Z., Rahman, N.S.S.A., Sarijo, S.H., Zainal, Z., 2011. Synthesis of a dual herbicides- intercalated layered zinc hydroxide nanohybrid with simultaneous controlled release property of the two herbicides. Int. J. Mol. Sci. 13, 7328–7342.

Jaerger, S., Zimmermann, A., Zawadzki, S.F., Wypych, F., Amico, S. C., 2014. Zinc layered hydroxide salts: intercalation and incorporation into low-density polyethylene. Polimeros 24, 683–688.

Lajmanovich, R.C., Junges, C.M., Attademo, A.M., Peltzer, P.M., Cabagna-Zenklusen, M.C., Basso, A., 2013. Individual and mixture toxicity of commercial formulations containing glyphosate, metsulfuron-methyl, bispyribac-sodium, and picloram on rhinella arenarum tadpoles. Water. Air. Soil Pollut. 224.

Li, B., He, J., Evans, D.G., 2008a. Experimental investigation of sheet flexibility of layered double hydroxides: one-pot morphosynthesis of inorganic intercalates. Chem. Eng. J. 144, 124–137.

Li, J., Li, Y., Dong, H., 2008b. Controlled release of herbicide acetochlor from clay/carboxylmethylcellulose gel formulations. J. Agric. Food Chem. 56, 1336–1342.

Liang, C., Tian, Z., Tsuruoka, T., Cai, W., Koshizaki, N., 2011. Blue and green luminescence from layered zinc hydroxide/dodecyl sulfate hybrid nanosheets. J. Photochem. Photobiol. A Chem. 224, 110–115.

Liu, J., Zhang, X., Zhang, Y., 2015. Preparation and release behavior of chlorpyrifos adsolubilized into layered zinc hydroxide nitrate intercalated with dodecylbenzenesulfonate. ACS Appl. Mater. Interfaces 7, 11180–11188.

Lucinda-Silva, R.M., Salgado, H.R.N., Evangelista, R.C., 2010. Alginate-chitosan systems: in vitro controlled release of triamcinolone and in vivo gastrointestinal transit. Carbohydr. Polym. 81, 260–268.

Mac Hado, G.S., Arízaga, G.G.C., Wypych, F., Nakagaki, S., 2010. Immobilization of anionic metalloporphyrins on zinc hydroxide nitrate and study of an unusual catalytic activity. J. Catal. 274, 130–141.

Moezzi, A., Cortie, M., McDonagh, A.M., 2013. Formation of zinc hydroxide nitrate by H + -catalyzed dissolution-precipitation. Eur. J. Inorg. Chem., 1326–1335

Nhlapo, N., Motumi, T., Landman, E., Verryn, S.M.C., Focke, W.W., 2008. Surfactant-assisted fatty acid intercalation of layered double hydroxides. J. Mater. Sci. 43, 1033–1043.

Pesquisa, C. De, Cepesq, A., Química, D. De, 2015. Layered zinc hydroxide salts intercalated with anionic surfactants and adsolubilized with UV absorbing organic. Molecules 26, 1769–1780.

Qamruzzaman, Nasar, A., 2019. Degradative treatment of bispyribac sodium herbicide from synthetically contaminated water by colloidal MnO2 dioxide in the absence and presence of surfactants. Environ. Technol. (United Kingdom) 40, 451–457.

Qiu, D.P., Hou, W.G., Xu, J., Liu, J., Liu, S., 2009. Synthesis and characterization of imidacloprid/hydrotalcite-like compound nanohybrids. Chinese J. Chem. 27, 1879–1885.

Rana, D., Bag, K., Bhattacharyya, S.N., Mandal, B.M., 2000. Miscibility of poly(styrene-co-butyl acrylate) with poly(ethyl methacrylate): existence of both UCST and LCST. J. Polym. Sci. Part B Polym. Phys. 38, 369–375.

Rana, D., Mandal, B.M., Bhattacharyya, S.N., 1996a. Analogue calorimetry of polymer blends: poly(styrene-co-acrylonitrile) and poly(phenyl acrylate) or poly(vinyl benzoate). Polymer (Guildf) 37, 2439–2443.

Rana, D., Mandal, B.M., Bhattacharyya, S.N., 1996b. Analogue calorimetric studies of blends of poly(vinyl ester)s and polyacrylates. Macromolecules 29, 1579–1583.

Rana, D., Mandal, B.M., Bhattacharyya, S.N., 1993. Miscibility and phase diagrams of poly(phenyl acrylate) and poly(styrene-co-acrylonitrile) blends. Polymer (Guildf) 34, 1454–1459.

Rees, J.R., Burden, C.S., Fogg, A.M., 2014. New layered double hydroxides by prepared by the intercalation of gibbsite. J. Solid State Chem., 1–4

Ribeiro, L.N.M., Alcântara, A.C.S., Darder, M., Aranda, P., Araújo-Moreira, F.M., Ruiz-Hitzky, E., 2014. Pectin-coated chitosan-LDH bionanocomposite beads as potential systems for colon-targeted drug delivery. Int. J. Pharm. 463, 1–9.

Rives, V., Ulibarri, M.A., 1999. Layered double hydroxides (LDH) intercalated with metal coordination compounds and oxometalates. Coord. Chem. Rev. 181, 61–120.

Ruiz de Arcaute, C., Soloneski, S., Larramendy, M.L., 2016. Toxic and genotoxic effects of the 2,4-dichlorophenoxyacetic acid (2,4-D)-based herbicide on the Neotropical fish Cnesterodon decemmaculatus. Ecotoxicol. Environ. Saf. 128, 222–229.

Sarijo, S.H., Ghazali, S.A.I.S.M., Hussein, M.Z., Ahmad, A.H., 2015. Intercalation, physicochemical and controlled release studies of organic-inorganic–herbicide (2,4,5 tricholorphenoxy butyric acid) nanohybrid into hydrotalcite-like compounds. Mater. Today Proc. 2, 345–354.

Shulman, G.P., Simmonds, P.G., 1968. Thermal decomposition of aromatic and heteroaromatic amino-acids. Chem. Commun. 17, 1040–1042.

Sing, K.S.W., 1985. Physical and biophysical chemistry division commission on colloid and surface chemistry including catalysis. Pure Appl. Chem. 57, 603–619.

Soledad, M., Román, S., Holgado, M.J., 2015. Intercalation of phenylalanine, isocoumarin and ochratoxin A (OTA) into LDH's. 52–62.

Tao, Q., Yuan, J., Frost, R.L., He, H., Yuan, P., Zhu, J., 2009. Effect of surfactant concentration on the stacking modes of organosilylated layered double hydroxides. Appl. Clay Sci. 45, 262–269.

Toni, C., de Menezes, C.C., Loro, V.L., Clasen, B.E., Cattaneo, R., Santi, A., Pretto, A., Zanella, R., Leitemperger, J., 2010. Oxidative stress biomarkers in Cyprinus carpio exposed to commercial herbicide bispyribac-sodium. J. Appl. Toxicol. 30, 590–595.

Touloupakis, E., Margelou, A., Ghanotakis, D.F., 2011. Intercalation of the herbicide atrazine in layered double hydroxides for controlled-release applications. Pest Manag. Sci. 67, 837–841.

Woranuch, S., Yoksan, R., 2013. Eugenol-loaded chitosan nanoparticles: I. Thermal stability improvement of eugenol through encapsulation. Carbohydr. Polym. 96, 578–585.

Zhang, Q., Zhao, Y., Fan, S., Bai, A., Li, X., Pan, C., 2013. Dissipation and residues of bispyribac-sodium in rice and environment. Environ. Monit. Assess. 185, 9743–9749.

Zhenlan, Q., Heng, Y., Bin, Z., Wanguo, H., 2009. Synthesis and release behavior of bactericides intercalated Mg-Al layered double hydroxides. Colloids Surf. A Physicochem. Eng. Asp. 348, 164–169.